Surface relaxation effects on the properties of porous silicon

E. Vázquez, and J. Tagüeña-Martínez[a)]
Centro de Investigación en Energia, Universidad Nacional Autónoma de México, Apartado Postal 34, Temixco, 62580 Morelos, México

L. E. Sansores, and C. Wang
Instituto de Investigaciones en Materiales, Universidad Nacional Autónoma de México, Apartado Postal 70-360, 04510, México D. F., México

(Received 14 March 2001; accepted for publication 5 December 2001)

In this article, surface relaxation and its effects on the electronic and structural properties of porous silicon are studied by using the total-energy pseudopotential formalism within the density-functional theory. Our model is based on a 32-atom supercell, where columns of atoms are removed and saturated with hydrogen atoms. Samples with 4.4%, 13.6%, 16.8%, 28.9%, and 41.3% porosity are analyzed in detail. The results show a clear expansion of the system along the pore direction as the porosity increases. Moreover, this expansion is very sensitive to the hydrogen-atom concentration and a linear dependence is observed. The dependence of the band gap and the effective mass on the porosity are also analyzed. Here, the hydrogen-atom number and pore shapes are observed to play a fundamental role. © *2002 American Institute of Physics.* [DOI: 10.1063/1.1446658]

I. INTRODUCTION

Porous silicon (por-Si) has been studied extensively for the last ten years, since the discovery of its efficient visible luminescence at room temperature.[1] The optical properties of por-Si are quite different from those of crystalline silicon (c-Si). It has been suggested that quantum confinement and surface effects are behind this difference. Recent experiments using x-ray techniques have shown an increase in the lattice parameter perpendicular to the pore-growing surface. Buttard *et al.*,[2] studying por-Si samples with porosities ranging between 35% and 84%, found an increase in the lattice parameter along the normal direction of the sample surface as the porosity increases. Grüning *et al.*[3] studied mechanical stress during the drying of por-Si and observed an increase in $\Delta c/c$ of between 10^{-4} and 10^{-3} after the process for samples prepared from p^+ silicon, and of a few parts per thousand in samples prepared from p^- silicon. Sugiyama and Nittolo[4] also report an increase in the lattice parameter in their samples after annealing.

Two theoretical models have been proposed to investigate the properties of this material: isolated Si quantum wires and columnar pores. Semi-empirical[5–8] and first-principles local-density[9–12] calculations have been performed within the first model, while the second one is not so widely used although it has the advantage of being able to incorporate the interconnectivity of the system. When the columnar pores are distributed periodically, it is called the supercell model and it has been used by Cruz *et al.*[13] within the tight-binding approximation.

The aim of this work is to combine the supercell model and a first-principles calculation to understand the effects of surface relaxation on the structural and optical properties of por-Si. An interesting comparison is made with results obtained from the quantum wire model. The computational method is an *ab initio* total energy pseudopotential technique within the density functional theory (DFT) in the generalized gradient approximation (GGA), as implemented in the CASTEP code.[14]

II. MODEL AND THE COMPUTATIONAL DETAILS

Starting from an eight-atom cubic unit cell of Si, we construct a 32-atom supercell by taking two units in the a and b directions. The structure of this supercell has been optimized to have a fully relaxed unit cell with a $P1$ symmetry. From this starting point, we generate four different samples removing columns of 1, 4, 5, 9, and 13 atoms of Si in the c ([001]) direction, producing samples with 4.4%, 13.6%, 16.8%, 28.9%, and 41.3% porosity, respectively. These samples have been built removing neighboring columns of atoms, but in the four-atom case, the second-neighbor columns are involved, producing more dangling bonds per column of atoms removed. In this work, the porosity (p) is defined as the ratio $p=(\rho_{\text{por-Si}}/\rho_{c\text{-Si}})\times 100$, where $\rho_{\text{por-Si}}$ and $\rho_{c\text{-Si}}$ are the densities of the porous and crystalline silicon samples, respectively. It would be worth mentioning that the samples with 13.6% and 28.9% porosity require a higher number of hydrogen atoms to saturate the dangling bonds. After creating the pores, we introduce hydrogen atoms to saturate the dangling bonds of the Si on the surface of the pores. An initial relaxation with molecular mechanics has been done allowing only the hydrogen atoms to move.

The calculations have been carried out using the CASTEP codes developed at Cambridge University.[15] The program uses the density-functional framework[16] with local density approximation (LDA)/GGA for exchange and correlation,[17,18] and norm-conserving, nonlocal, Troullier–Martins pseudopotentials[19] generated by the Kerker method.[20] The electronic wave functions are expanded in a

a)Electronic mail: jtag@servidor.unam.mx

TABLE I. Parameters used in the calculations.

Sample	Si	SiP 1 Hr	SiP 4 Hr	SiP 5 Hr	SiP 9 Hr	SiP 13 Hr	Q. wire
k points	4×4×4	2×2×2	2×2×2	2×2×2	2×2×2	2×2×2	2×2×2
Plane waves	11 099	39 240	39 240	39 808	39 240	40 565	74 871
Fourier-Transform grid	54×54×27	80×80×40	80×80×40	80×80×40	80×80×40	80×80×45	120×120×40
E_{cut}(eV)	400	900	900	900	900	900	900
Lattice	P1 triclinic	P1 triclinic	P1 triclinic	P1 triclinic	P1 triclinic	P1 triclinic	P1 triclinic
a	10.8	10.86	10.86	10.86	10.86	10.86	15
c	5.4	5.4388	5.4668	5.504 15	5.501 68	5.611 998	5.429 21
No. Si	32	31	28	27	23	19	9
No. H	0	4	8	12	12	20	12
ρ (g/cm^3)	2.369	2.268	2.046	1.998	1.706	1.436	0.36
d (%)	0	4.4	13.6	16.8	28.9	41.3	86.7

plane wave basis set with periodic boundary conditions and a plane wave energy cutoff. In all cases, the Monkhorst–Pack method[21] has been used to select the **k** points set, with a 4×4×4 grid for the small unit cell of *c*-Si and a 2×2×2 grid for the supercells of our por-Si samples. Parameters for the calculations are given in Table I. Two different cutoff energies have been used. For the *c*-Si, the cutoff was set at 400 eV, while for all the por-Si samples, it was set at 900 eV. This last value is due to the presence of hydrogen atoms. In all cases, convergence was checked by increasing the cutoff and **k** point grid for some samples.

A full geometry optimization has been done within the DFT by fixing the angles and the parameters *a* and *b* of the unit cell, allowing relaxation of the parameter *c* and the atomic positions. These restrictions are considered since it is experimentally known that the crystal structure of por-Si is the same as that of *c*-Si and that only the cell parameter perpendicular to the growth surface changes. Final cell parameters are given in Table I and some structures are shown in Fig. 1.

Finally, calculations have also been performed for a periodic model of quantum wires. In this case, we start from the same supercell of 32 atoms and remove columns of atoms in the *c* direction to form an isolated quantum wire of nine atoms. The surface of the wire is saturated with hydrogen, taking especial care that the hydrogen atoms are directed toward the outside of the wire. The wire diameter is 5.43 Å and the shortest distance between the H atoms in different wires is 8.070 Å. In Fig. 2, the quantum wire used is shown from two different angles of view. It corresponds to a 86.7% porosity. The same relaxation procedure as before was followed here.

III. RESULTS

The surface relaxation process leads the atoms to their thermodynamical equilibrium positions, releasing the internal stress in the por-Si samples. During relaxation, the total energy decreases while the electronic band gap increases. The relaxed electronic bands are flattened, and consequently the effective mass increases. In Fig. 3(a), the change in the parameter *c* (Δc, the difference between the relaxed and the nonrelaxed structure) as a function of the porosity is plotted. The general trend is that Δc rises as the porosity increases, except in the samples with 16.8% and 28.9% porosities which have almost the same Δc. If instead of the porosity we plot Δc as a function of the hydrogen content as shown in Fig. 3(b), a linear behavior is obtained. This behavior, as well as the magnitude of Δc are in agreement with the experimental results of Barla *et al.*,[22] who report an increase in the lattice parameter when the samples are dried in air, and an larger increase when they are soaked in pentane. When the pentane is applied after the anodic reaction, it reduces the number of Si—O bonds allowing an increase of the Si—H bonds. Hydrogen covered surfaces are known to be mutually attracted, due to van der Waals forces, which are therefore expected to contribute to the overall stress and the surface tension.[3] Due to a minimization of the surface (note the tendency to circular pores in Fig. 1), the hydrogen confined in

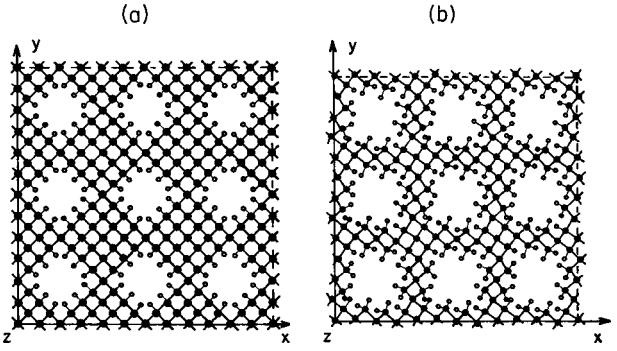

FIG. 1. Front view of (a) 28.9% porosity supercell saturated with 12 hydrogen atoms (open circles) and (b) 41.3% porosity with 20 hydrogen atoms.

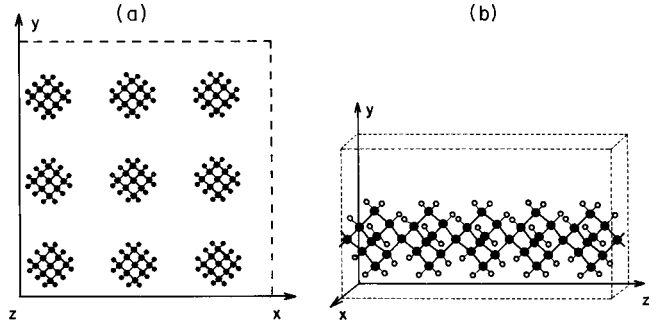

FIG. 2. (a) Front and (b) side views of a quantum wire used in our calculations.

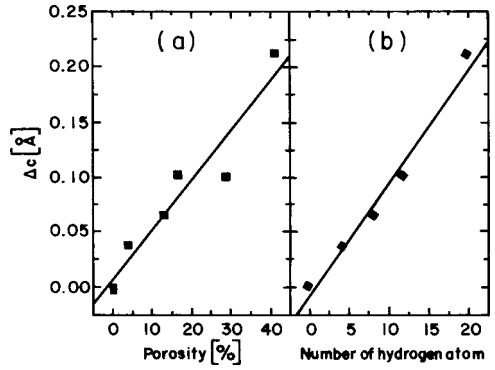

FIG. 3. Changes of the lattice parameter Δc (a) as a function of the porosity, and (b) as a function of the hydrogen content, i.e., the number of hydrogen atoms used to saturate the pore surface.

the pore will push to expand the Si structure in the [001] direction. As the size of the pores grows, more hydrogen atoms are needed to saturate the broken bonds, and a stronger expansion of the structure is observed.

As seen in Table II, our calculations on the quantum wire show that, in this case, the lattice parameter c decreases, $\Delta c = -0.008$ Å, when the saturating hydrogen atoms are oriented toward the outside of the wire. This behavior is in disagreement with experimental results. It is worth mentioning that if the hydrogen atoms saturating the surface are embedded in the wire, their effect will be to increase the c parameter.

On the other hand, the electronic band structures obtained from the five samples of por-Si discussed before have been calculated in the [010], [$0\frac{1}{2}1$], [$01\frac{1}{2}$], [$11\frac{1}{2}$], and [111] directions in **k** space. In particular, band structures for 13.6% and 41.3% porosity are shown in Figs. 4(a), and 4(b). The general behavior shows that as the porosity increases, the bands become flat. This effect is first seen on the conduction bands at low porosity. As porosity increases, the valence bands also flatten. Table III summarizes the results of the band structure analysis. As expected, this flattening is stronger near the band gap, but for high porosity, all calculated bands become planar.

Both the lower conduction and the upper valence band edges shift linearly as porosity increases, but the latter decreases faster, as shown in Fig. 5(a). The net effect is that the band gap (E_g) increases linearly with the porosity as seen in Fig. 5(b). This behavior is in agreement with the experimental work of Lugo *et al.*,[23] where a linear relationship between the effective absorption coefficient and the porosity is obtained. The energy shift of around 5 eV must be reflected in the value of the work function. Experimentally,[24] an increase in the work function is found as the porosity increases. However, the large value of the change in energy is probably due to a decrease in the number of silicon atoms.

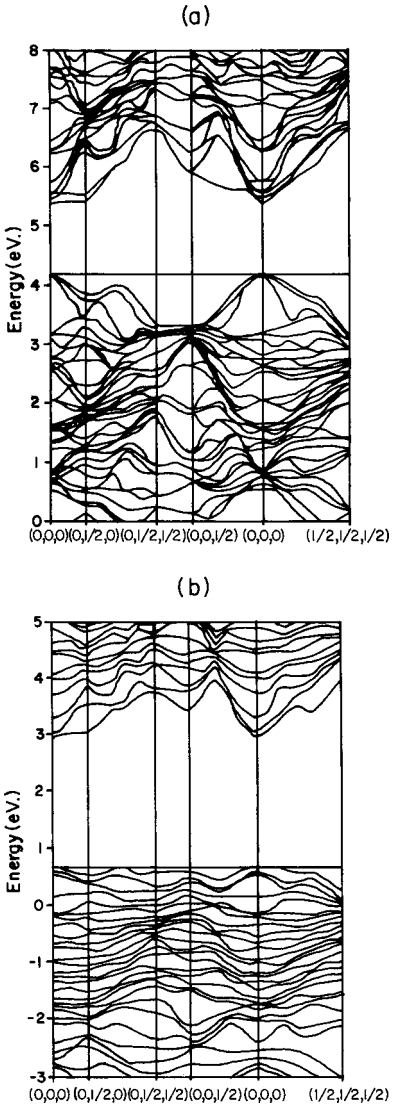

FIG. 4. Electronic band structures of (a) the 13.6% porosity sample of por-Si, and (b) the 41.3% porosity sample of por-Si.

To analyze the confinement effect, we have defined the confinement distance d as the diagonal separation between pores shown in Fig. 6, and if we assume that $E_g \sim d^{\alpha}$, we obtain $\alpha = -1.78$. Experimental attempts to find a value of α

TABLE II. absolute (Δc) and relative ($\Delta c/c$) changes in lattice parameter c calculated for different porosity (p) and number of hydrogen atoms ($n_{\mathbf{H}}$).

Sample	p (%)	Δc (Å)	$\Delta c/c$	n_{H}
SiP 1 Hr	4.4	0.0388	0.007 14	4
SiP 4 Hr	13.6	0.0668	0.012 30	8
SiP 5 Hr	16.8	0.104 148	0.019 18	12
SiP 9 Hr	28.9	0.101 682	0.018 72	12
SiP 13 Hr	41.3	0.211 998	0.039 04	20
Q. wire	86.7	−0.000 787	-1.45×10^{-4}	12

TABLE III. Electronic band structure parameters: porosity (p), band gap (E_g), normalized effective mass (m_h/m_0), and confinement distance (d).

Sample	p (%)	Gap type	E_g (eV)	m_h/m_0	d
Silicio	0	Indirect	0.61	0.87	0.0
SiP 1 Hr	4.4	Direct	0.77	0.91	11.18
SiP 4 Hr	13.6	Direct	1.19	1.23	9.46
SiP 5 Hr	16.8	Indirect	1.31	1.72	7.49
SiP 9 Hr	28.9	Indirect	1.80	2.62	7.47
SiP 13 Hr	41.3	Direct	2.29	3.21	3.72

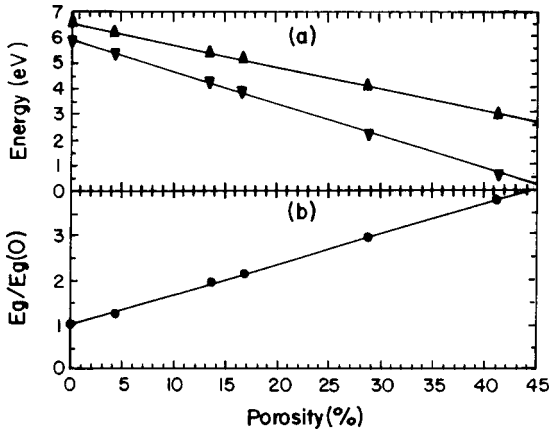

FIG. 5. (a) Lower conduction (solid up triangles) and upper valence (solid down triangles) band edges and (b) band gap (E_g), both as a function of the porosity.

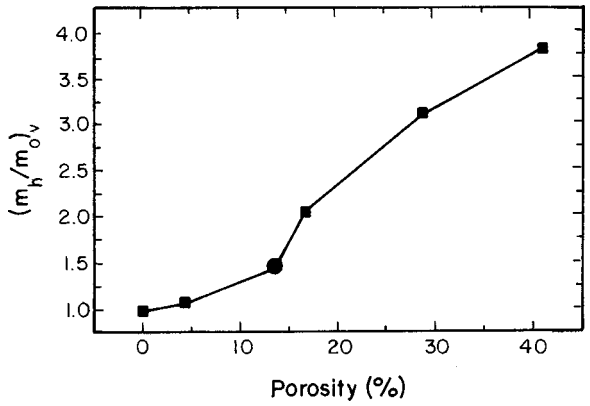

FIG. 7. Valence band effective mass as a function of the porosity. The 13.6% porosity sample has a different morphology and thus a different behavior (indicated by a bigger solid circle).

have not been conclusive due to the inhomogeneity of the pores and the difficulty in measuring the confinement distance.[25] On the theoretical side, strong coupling results predict $\alpha = -1.39$. Other calculations using experimental results show a complicated dependence.[26] It should be noted that our work is also not conclusive.

With respect to the effective mass in the valence band, we have found that it increases with the porosity, as shown in Fig. 7. At low porosity, 4.4%, the change is very small. As the porosity increases, the change in effective mass grows also, being approximately linear for porosities above 16.8%. Our results also show the importance of pore symmetry on effective mass. It can be seen that the effective mass for the pore with a different symmetry (indicated by a circle in Fig. 7 and discussed in the previous section) has a slightly different behavior. Here, although the general trend is in agreement with experimental results, the increase in m_h starts at lower porosity than reported experimentally.[27] It is worth mentioning that the changes with porosity in the band dispersion and in the effective mass are consistent and highly related, as would be expected.

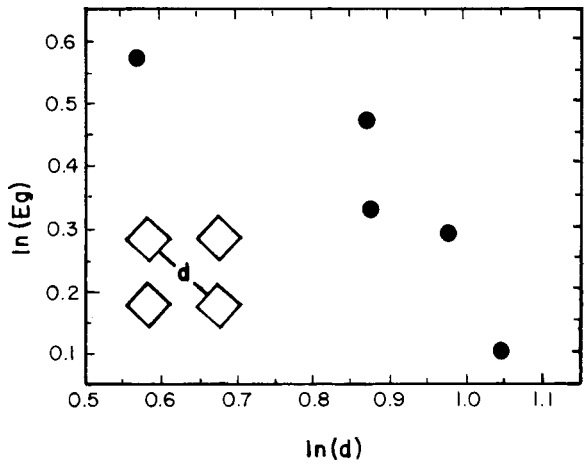

FIG. 6. Plot of $\ln(E_g)$ vs $\ln(d)$, where d(Å) is the confinement distance between pores defined in the insert.

IV. CONCLUSIONS

We have studied surface relaxation and its effects on the electronic and structural properties of porous silicon by using the total-energy pseudopotential formalism within the DFT. The results show that regarding the change in the lattice parameters, the supercell model is more adequate than the quantum-wire model for describing por-Si. Furthermore, the effects of saturation and relaxation of the pore surface should be considered if one wishes to obtain an adequate description the properties of por-Si. The results also show that not only the porosity but also the morphology and symmetry of the pores are important. In particular, the lattice parameter c correlates better with the number of hydrogen atoms than with the size of the pore, which can be explained in terms of a minimization of the surface. This fact is in agreement with the experimental work of Barla *et al.*[22]

On the other hand, an increase in the work function is predicted in agreement with experimental data. At low porosity (4.4%), the conduction bands near the gap begin to flatten. As the porosity increases, this band flattening is induced in bands farther away from the gap. The same effect is seen in the valence bands, but a higher porosity is needed to have a notable effect. At high porosity, all the bands flatten. The effective mass in the valence band increases very slowly at low porosity and faster at high porosity.

Finally, we should note that our results of Δc agree with the experimental ones. However, we cannot quantitatively reproduce the band gap of por-Si, as it is well known that DFT-LDA largely underestimates the band gap values since the many-body effects are not properly considered. Other sources of error are the limited size of samples and the periodic nature of the supercell model.

ACKNOWLEDGEMENTS

This work was partially financed by CONACYT Project No. 32148E and DGAPA Project Nos. IN101100 and IN101701. The authors wish to acknowledge the help of Dirección General de Cómputo Académico for computer time on the Origin 2000, and of Dr. A. Mehta for the critical reading of the manuscript.

[1] L. T. Canham, Appl. Phys. Lett. **57**, 1046 (1990).
[2] D. Buttard, D. Bellet, and G. Dolino, J. Appl. Phys. **83**, 5814 (1998).
[3] U. Grüning and A. Yelon, Thin Solid Films **255**, 135 (1995).
[4] H. Sugiyama and O. Nittono, J. Cryst. Growth **103**, 156 (1990).
[5] G. D. Sanders and Y.-C. Chang, Phys. Rev. B **45**, 9202 (1992).
[6] C. Delerue, G. Allan, and M. Lannoo, Phys. Rev. B **48**, 11024 (1993).
[7] C.-Y. Yeh, S. B. Zhang, and A. Zunger, Appl. Phys. Lett. **63**, 3455 (1993).
[8] H. M. Polatoglou, J. Lumin. **57**, 117 (1993).
[9] A. J. Read, R. J. Needs, K. J. Nash, L. T. Canham, P. D. J. Calcott, and A. Qteish, Phys. Rev. Lett. **69**, 1232 (1992).
[10] F. Buda, J. Kohanoff, and M. Parrinello, Phys. Rev. Lett. **69**, 1272 (1992).
[11] T. Ohno, K. Shiraishi, and T. Ogawa, Phys. Rev. Lett. **69**, 2400 (1992).
[12] M. S. Hybertsen and M. Needels, Phys. Rev. B **48**, 4608 (1993).
[13] M. Cruz, C. Wang, M. R. Beltran, and J. Tagüeña-Martínez, Phys. Rev. B **53**, 3827 (1996).
[14] M. C. Payne, M. P. Teter, D. C. Allan, T. A. Arias, and J. D. Joannopoulos, Rev. Mod. Phys. **64**, 1045 (1992).
[15] Cerius^2 User Guide, Month 1994. (Molecular Simulation, Inc. San Diego 1997).
[16] W. Kohn and L. J. Sham, Phys. Rev. A **140**, 1133 (1965).
[17] J. P. Perdew and A. Zunger, Phys. Rev. B **23**, 5048 (1981).
[18] D. M. Ceperley and B. J. Alder, Phys. Rev. Lett. **45**, 566 (1980).
[19] N. Troullier and J. L. Martins, Phys. Rev. B **43**, 1993 (1991).
[20] G. P. Kerker, J. Phys.: Condens. Matter **13**, L189 (1980).
[21] H. J. Monkhorst and J. D. Pack, Phys. Rev. B **13**, 5188 (1976); J. D. Pack and H. J. Monkhorst, *ibid.* **16**, 1748 (1977).
[22] K. Barla, G. Bomchil, R. Herino, J. C. Pfister, and J. Baruchel, J. Cryst. Growth **68**, 727 (1984).
[23] J. E. Lugo, J. A. del Rio, and J. Tagüeña-Martinez, J. Appl. Phys. **81**, 1923 (1997).
[24] T. M. Bhave and S. V. Bhoraskar, J. Vac. Sci. Technol. B **16**, 2073 (1998).
[25] S. Schupplet, *et al.*, Phys. Rev. B **52**, 4910 (1995).
[26] Properties of Porous Silicon, edited by L. Canham (IEEE, London, 1997), p. 207.
[27] I. Sagnes, A. Halimaoui, G. Vincent, and P. A. Badoz, Appl. Phys. Lett. **62**, 1155 (1993).